Eur Biophys J (2011) 40:1205–1214
DOI 10.1007/s00249-011-0742-z

ORIGINAL PAPER

EBSA
Biophysics in Europe

Cis–trans photoisomerization properties of GFP chromophore analogs

Gerardo Abbandonato · Giovanni Signore · Riccardo Nifosì · Valerio Voliani · Ranieri Bizzarri · Fabio Beltram

Received: 11 March 2011 / Accepted: 9 August 2011 / Published online: 31 August 2011

Abstract The photoswitching behaviour of the green fluorescent protein (GFP) chromophore and its analogs opens up exciting horizons for the engineering and development of molecular devices for high sensitivity in vivo studies. In this work we present the synthesis and photophysical study of four GFP chromophore analogs belonging to butenolide and pyrrolinone classes. These chromophores possess an intriguing photoinduced *cis–trans* isomerization mechanism. Stereochemical structural assignment was unambiguously performed by 1D Nuclear Overhauser Effect NMR measurements. The spectroscopic properties of both *cis* and *trans* isomers were studied, and photoconversion quantum yield for *cis–trans* isomerization was assessed to be in the 0.1–0.4 range. Finally, the $^{3}J_{C,H}$ coupling constant in the ^{13}C–C=C–H motif was in excellent agreement with theoretical DFT calculations, thus providing a further confirmation of *cis–trans* photoisomerization of the structurally analog GFP chromophore.

Keywords GFP chromophore · Photoswitching · *Cis–trans* isomerization · $^{3}J_{C,H}$ coupling · 1D-NOE

Special Issue: SIBPA 2011 Meeting.

G. Abbandonato · V. Voliani · R. Bizzarri (✉) · F. Beltram
NEST, Scuola Normale Superiore, Piazza San Silvestro 12, 56127 Pisa, Italy
e-mail: r.bizzarri@sns.it

G. Abbandonato · G. Signore · V. Voliani · R. Bizzarri · F. Beltram
Center for Nanotechnology Innovation @NEST, Istituto Italiano di Tecnologia, Piazza San Silvestro 12, 56127 Pisa, Italy

R. Nifosì · R. Bizzarri · F. Beltram
NEST, Istituto Nanoscienze, Consiglio Nazionale delle Ricerche, Piazza San Silvestro 12, 56127 Pisa, Italy

Introduction

Photoinduced alterations of physicochemical properties of organic molecules are increasingly studied in view of engineering new photoresponsive nanodevices tailored to different applications. Among others, optically bistable (referred to as photochromic or photoswitchable) molecules are particularly promising for the real-time fluorescence imaging of biological samples at the nanoscale. Indeed, a wide range of techniques (Betzig et al. 2006; Hell 2007; Hess et al. 2006; Rust et al. 2006) exploit the light-driven saturable optical transitions between the two states of a photochromic fluorescent probe [a process generally denoted as RESOLFT (Schwentker et al. 2007)] to break the light's diffraction barrier and image living matter at the nanoscale by means of optical microscopy setups (Hell 2009). Photoswitchable molecules can also be fruitfully used as part of fluorescent indicators based on the resonance energy transfer between two optically complementary molecules: photoswitching allows modulating the energy transfer process temporally, thereby increasing the measurement sensitivity (Bizzarri et al. 2010; Yan et al. 2011). Finally, reversible photoswitching can be used to address sequentially different sample regions in fluorescent microscopy (Ando et al. 2004).

Nature is a continuous source of inspiration for the design of photoactive molecules, owing to the widespread use of photoinduced processes in living organisms. Autofluorescent proteins (AFP), originally derived from sea organisms, constitute the family of the most popular fluorescent probes for intracellular microscopy studies owing to their genetic encoding of fluorescence (Stepanenko et al. 2008). Recently, the efficient *cis–trans* photoisomerization of the internal chromophore has been described for several AFPs, and it is the basis for the reversibly photoswitchable

fluorescence of these fluorescent probes (Abbruzzetti et al. 2010; Ando et al. 2007; Andresen et al. 2007, 2008; Bizzarri et al. 2010; Fernandez-Suarez and Ting 2008; Luin et al. 2009). Actually, the *cis–trans* photoisomerization is an intrinsic hallmark of the imidazolinone AFP chromophore, as demonstrated by several groups including us (Dong et al. 2008; Voliani et al. 2008). It is worth noting that AFP synthetic chromophore analogs such as *p*-HBDI [the chromophore analog of archetype wild-type green fluorescent protein (Kojima et al. 1998; Niwa et al. 1996)] are characterized by a striking photoswitching yield of 0.1 and above (1 out of 10 absorbed photons activate photoswitching), whereas efficiencies two to three orders of magnitude lower are found in the corresponding proteins on account of the hampering effects of the protein tertiary structure on the photoisomerization process. Thus, AFP chromophore structures can be considered as a promising starting point for engineering new photochromic molecules working either in absorption or in fluorescence.

In this work, we focused on two butenolide (B1 and B2) and two pyrrolinone (P1 and P2, Scheme 1) derivatives that are related to AFP chromophores but contain an additional phenyl ring linked to the five-member heteroaromatic ring (Scheme 1). B2 and P2 differ from B1 and P1 by the presence of two electron-donating methyl ether groups in this second phenyl ring. Besides their peculiar electronic property, these groups are intended to mimic lateral chains for further chemical functionalization. A similar approach was recently followed by us in the design and development of solvatochromic coumarin probes (Signore et al. 2009, 2010).

The synthesis of these four compounds has been previously demonstrated to lead uniquely to the (*Z*)-isomer (Bourotte et al. 2004); however, no data on photoisomerization processes have been reported. Here, we demonstrate that these four compounds all undergo very effective

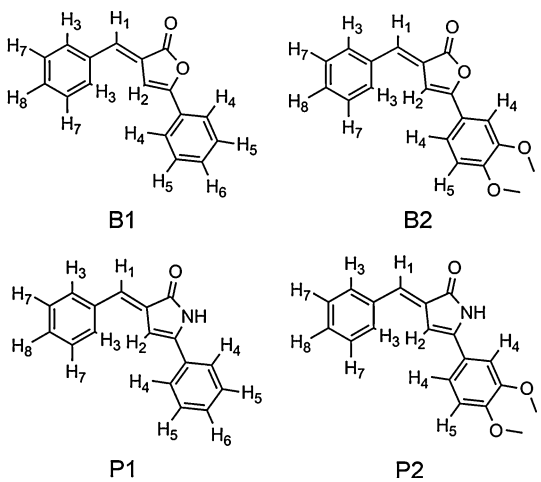

Scheme 1 Structures of chromophores B1, B2, P1 and P2

cis–trans photoisomerization associated with photoswitching yields comparable to AFP chromophore derivatives. Notably, the configurational assignment was carried out by structurally tailored NMR measurements and their interpretation in view of theoretical calculations. This strategy was indeed developed to allow for a prompt and general identification of photoisomerization characteristics in AFP chromophore analogs.

Materials and methods

Chromophore synthesis (Scheme 2)

The butenolide chromophores were synthesized according to the reported procedure that involves the cyclization of either 3-benzoylpropionic acid or 3-(3,4-dimethoxyphenyl)propionic acid upon reaction with stoichiometric benzaldehyde by heating with acetic anhydride, in the presence of sodium acetate. A mixture of 10 mmol of benzaldehyde, 10 mmol of 3-benzoylpropionic acid, 10 mmol of sodium acetate and 5 ml of acetic anhydride was heated under reflux until crystals separated. After cooling, the reaction was poured into water, and the solid product was filtered, washed with water and finally recrystallized from 95% ethanol. Pure products were easily obtained by filtration. Yields: 51% (B1), 46% (B2).

The pyrrolinone chromophores were synthesized from the butenolide analogs (0.7 mmol) in an MeOH suspension (5 ml) with 2 ml of 30% ammonia solution and 0.2 ml of glacial acetic acid, according the reported procedure. The mixture was stirred and heated under reflux for 5 h. The solution was evaporated to dryness, and CH_2Cl_2 (5 ml) was added. The solid product was filtered and washed with water. Yields: 31% (P1), 50% (P2).

Analytical data for the compound of butenolide class (B1 and B2) are as follows: B1: ^{1}H NMR (300 MHz, DMSO) δ 8.06 (bd, 4H, *H3, H4*), 7.81 (s, 1H, *H1*), 7.67 (bm, 6H, ArH), 7.57 (s, 1H, *H2*); ^{13}C NMR (75 MHz, DMSO) δ 169.43, 156.71, 135.86, 131.94, 131.34, 131.27, 129.82, 129.67, 129.14, 128.45, 126.01, 125.32, 101.82. B2: ^{1}H NMR (300 MHz, DMSO) δ 7.85 (bd, J = 7, 2H, *H3*), 7.46 (bm, 4H, ArH), 7.44 (s, 1H, *H1*), 7.42 (dd, $J_{H4H5} = 11$, $J_{H4H4'} = 2$, 1H, *H4*), 7.30 (s, 1H, *H2*), 7.07 (d, J = 11, 1H, *H5*), 3.85 (s, 3H, OC*H*$_3$), 3.81(s, 3H, OC*H*$_3$); ^{13}C NMR (75 MHz, DMSO) δ 169.67, 156.89, 151.81, 149.81, 135.34, 134.17, 131.12, 130.99, 129.81, 125.45, 120.98, 119.57, 112.46, 109.17, 100.02, 56.54, 56.36.

Analytical data for the compound of pyrrolinone class (P1 and P2) are as follows: P1: ^{1}H NMR (300 MHz, DMSO) δ 10.58 (bs, 1H, N*H*), 7.89 (bd, J = 7, 2H, *H3*), 7.83 (db, J = 7, 2H, *H4*), 7.45 (bm, 6H, ArH), 7.18 (s, 1H, *H1*), 6.91 (s, 1H, *H2*); ^{13}C NMR (75 MHz, DMSO)

Scheme 2 Synthetic strategy for the preparation of B1-2, P1-2

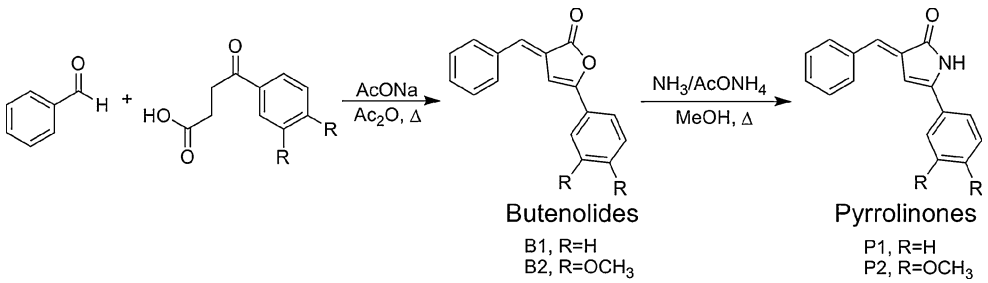

δ 171.58, 146.58, 136.09, 131.67, 130.97, 130.54, 130.35, 130.26, 130.08, 129.67, 129.44, 126.24, 97.95. P2:^{1}H NMR (300 MHz, DMSO) δ 10.66 (bs, 1H, N*H*), 7.95 (bd, J = 7, 2H, *H3*), 7.59 (bm, 5H, ArH), 7.24 (s, 1H, *H1*), 7.18 (dd, $J_{H4H5} = 11$, $J_{H4H4'} = 2$, 1H, *H4*), 6.94 (s, 1H, *H2*), 4.00 (s, 3H, OCH_3), 3.96 (s, 3H, OCH_3).

Upon photoconversion of the *cis* form of the chromophores, the following ^{1}H NMR spectra were recorded for the *trans* forms: B1 *trans* ^{1}H NMR (300 MHz, DMSO) δ 8.30 (bd, 4H, *H3*), 7.90 (bd, 4H, *H4*), 7.64 (bm, 6H, ArH and *H1*), 7.19 (s, 1H, *H2*); B2 *trans*: ^{1}H NMR (300 MHz, DMSO) δ 8.11 (bd, J = 7, 2H, *H3*), 7.46 (bm, 4H, ArH), 7.34 (s, 1H, *H1*), 7.27 (dd, $J_{H4H5} = 11$, $J_{H4H4'} = 2$, 1H, *H4*), 7.06 (d, J = 11, 1H, *H5*), 6.94 (s, 1H, *H2*), 3.82 (s, 3H, OCH_3), 3.80 (s, 3H, OCH_3); P1 *trans*:^{1}H NMR (300 MHz, DMSO) δ 10.58 (bs, 1H, N*H*), 8.33 (bd, J = 7, 2H, *H3*), 7.74 (bd, J = 7, 2H, *H4*), 7.42 (bm, 6H, ArH), 7.14 (s, 1H, *H1*), 6.39 (s, 1H, *H2*); P2 *trans*: ^{1}H NMR (300 MHz, DMSO) δ 10.48 (bs, 1H, N*H*), 8.30 (bd, J = 7, 2H, *H3*), 7.30 (bm, 5H, ArH), 7.03 (s, 1H, *H1*), 7.01 (d, J = 1, 1H, *H4*), 6.28 (s, 1H, *H2*), 3.81 (s, 3H, OCH_3), 3.78 (s,3H, OCH_3).

Absorption spectroscopy and photoconversion experiments

Ultraviolet-visible (UV-vis) spectra were measured on a Jasco 550 spectrometer (Jasco, Tokyo, Japan) supplied with a Jasco ETC-505T thermostat.

For photoconversion experiments, solutions of chromophore in organic solvents were placed in 1,500 µl quartz cells with a 1 cm path length. In all cases the solution optical density ranged between 0.05 and 0.1 Steady-state photoconversion was carried out by adopting a front-face illumination geometry while the solution was stirred continuously. Illumination at 405 nm was provided by a diode laser (FP-40/7AF-AV-SD5, Laser Components, Chelmsford, Essex, UK). An Ar laser (Stellar-PRO Select 150, Modu-Laser, South Centerville, UT) provided excitation illumination at 458 nm. Illumination power was kept below 0.5 mW to ensure photoswitching kinetics in the time scale of seconds.

Photoconversion of concentrated chromophore solutions (1–10 mM) in deuterated solvents was carried out by using an Ar-Kr laser (Beamlok 2060, Spectra Physics, Mountain View, CA) at 70 mW illumination power for times ranging between 10 and 30 min. Solutions at photosteady state were then diluted in selected, non-deuterated solvents down to an optical density of about 0.05–0.1 (usually 1/100 dilution) to obtain the absorption spectra of the photoconverted compounds.

NMR spectrometry

NMR spectra were collected by Varian Unity 300 spectrometer (Varian, Palo Alto, CA, USA) at room temperature on solutions in DMSO-d_6, acetonitrile-d_3 or $CDCl_3$.

^{1}H NMR spectra were collected at 300 MHz with the following experimental conditions: 23,998 points, 6 kHz of spectral width, 70° pulse, 2 s acquisition time and 200 transients. ^{13}C NMR spectra were collected at 75 MHz with the following experimental conditions: 72,008 points, 18 kHz of spectral width, 70° pulse, 2 s acquisition time and (1–6) $\times$ 10^5 transients. ^{1}H NMR steady-state NOE difference experiments were collected with the Cyclenoe pulse sequence with the following experimental conditions: 23,998 points, 6 kHz of spectral width, 90°, 2 s acquisition time and 200 transients, satpwr = −16, sattime = 5.

DFT calculations

DFT calculations were performed using the Gaussian 09 suite (Frisch et al. 2009). Molecular structures of the (*E*) and (*Z*) isomers were optimised at the DFT-B3LYP/6-31G(d) level. We adopted the small 6-31G(d) basis set only for geometry optimisation; we verified that this choice is reliable by comparing the results with those of larger basis sets. For the coupling constants, we employed the 6-311 ++G(d,p) basis set. B3LYP is known to have good performances for geometry optimisation of the kind of molecules studied in this work. NMR coupling constants were calculated using the Gauge-Independent Atomic Orbital (GIAO) method in the general framework of response theory (Helgaker et al. 2000), under the Gaussian09 keyword "nmr = spinspin" and with a 6-311 ++G(d,p) basis set. The reliability of the DFT/B3LYP approach for calculating coupling constants is also well established (Tripathi et al. 2007).

In the calculated J couplings, the Fermi contact term contributes more than 95%, the paramagnetic spin-orbit (PSO) and the spin-dipolar (SD) terms being negligible overall (<0.05 Hz), and the diamagnetic spin-orbit (DSO) term being on the order of a few tenths of Hz. Inclusion of implicit solvent effects through the polarizable continuum method (PCM) (Cossi and Barone 2001), either in structure optimisation or in the NMR calculations, resulted in differences of only 3% on the J couplings.

Results and discussion

Chromophore synthesis

Butenolides B1-2 as well as their corresponding pyrrolinonic isosteres P1-2 were synthesized according to a previously reported two-step procedure (Scheme 2; Schueler and Hanna 1951). Final yields ranged from 31 to 51%. NMR spectroscopic characterisation (see below) confirmed the pure (*Z*) stereochemical configuration of the synthesised molecules, as expected from the synthetic method (Bourotte et al. 2004). The presence of a sole *Z* isomer suggests that the thermodynamic stability of the corresponding E isomer is much lower and/or the energy barrier for the isomerization process is relatively high (note that the synthetic step was carried out at acetic anhydride reflux, i.e. 413 K). Consistently, in the following we shall show that the isomerization can be promoted by light absorption, but the thermal reaction is almost inhibited at room temperature. DFT calculations, by using B3LYP/6-31G(d) in DMSO with PCM (implicit solvent), allowed for the assessment of the relative stabilities of *Z* and *E* isomers. We found $\Delta G^0_{(Z-E)} = +2.23$ kcal/mol and +1.89 kcal/mol for the B1 and P1 compounds respectively. These figures indicate that the molar fractions of *Z* isomers are 2% (B1) and 4% (B2) at 298 K, too low to be detected by NMR.

For clarity, we hereafter shall refer to the (*Z*) and (*E*) isomers as *cis* and *trans*, respectively.

Optical properties of the chromophores

The UV-visible absorption spectra of *cis* chromophores are characterised by a broad band spanning the 350–500 nm interval and by a further band below 300 nm (Fig. 1a, b, blue lines). Analogously with the absorption spectra of *p*-HBDI, we may identify the band at lowest energy with the π-π^* transition (Voityuk et al. 1998). This transition appears the most relevant target for photoswitching experiments, in view of the possible incorporation of these chromophore units in fluorescent probes tailored to cell microscopy. We shall henceforth consider only this transition, which will be referred to as S0 → S1. Table 1 lists the peak maxima and extinction coefficients of S0 → S1 of

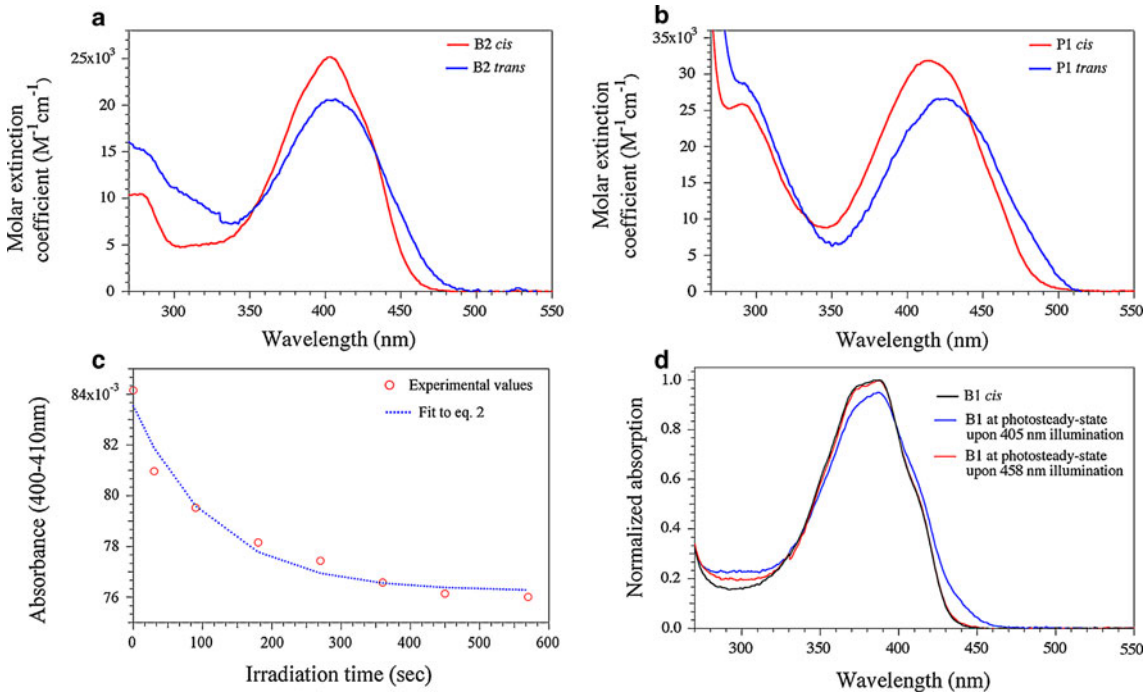

Fig. 1 **a** UV-vis spectra of *cis* (*red*) and *trans* (*blue*) isomers of B2, **b** UV-vis spectra of of *cis* (*red*) and *trans* (*blue*) isomers of P1, **c** photoconversion of P1 (*red circles*) upon irradiation at 405 nm, and fitting of the experimental data according to the adopted photokinetic model adopted (see text), **d** UV-vis spectra of pure *cis* B1 (*black line*), of B1 at photostationary state after irradiation at 405 nm (*blue line*), and at photosteady state after subsequent irradiation at 458 nm (*red line*)

Table 1 Photophysical properties of the S0 → S1 absorption transition of B1-2 and P1-2

	Acetonitrile		Isopropanol		CCl_4		AcOEt	
	Cis	*Trans*	*Cis*	*Trans*	*Cis*	*Trans*	*Cis*	*Trans*
B1								
ε_{max} ($M^{-1}cm^{-1}$)	38,500	38,600	32,600	20,200	27,700	18,800	32,500	14,800
λ_{max} (nm)	387.5	386	387	387.5	389.5	402	387.5	387
B2								
ε_{max} ($M^{-1}cm^{-1}$)	25,200	20,600	28,300	–	26,900	21,000	23,600	29,400
λ_{max} (nm)	403.5	406.5	403.5	–	405	416.5	404	404.5
P1								
ε_{max} ($M^{-1}cm^{-1}$)	21,000	17,500	14,000	6,000	16,000	13,200	18,600	10,500
λ_{max} (nm)	413.5	425	417	427	419.5	421.5	416.5	421
P2								
ε_{max} ($M^{-1}cm^{-1}$)	28,300	22,700	22,300	40,700	18,500	12,000	33,600	nd
λ_{max} (nm)	425.5	425.5	427.5	430	430	441.5	426.5	nd

cis chromophores in solvents with different polarity and H-bond capability; yet, the scarce solubility of these compounds in water prevented the investigation of such strong H-donor medium. Note that in all cases S0 → S1 was found to be associated to a significant extinction coefficient, falling in the 10,000–40,000 $M^{-1}cm^{-1}$ interval. S0 → S1 of *cis* pyrrolinones was red-shifted by 20–30 nm in comparison to *cis* butenolides (Table 1). The presence of electron-donating methyl ether groups in B2 and P2 further displaced S0 → S1 by 10–20 nm on the red side of the absorption compared to B1 and P1 (Table 1). The presence of an additional phenyl ring causes a significant red shift (about 15 and 40 nm for B1-2 and P1-2 respectively) of the S0 → S1 absorption transition with respect to the imidazolinone ring of *p*-HBDI. Taken together, these findings indicate the significant role of carefully selected groups in increasing electron delocalization over the aromatic rings. Interestingly, only a negligible effect of solvent polarity on peak wavelength could be observed, although the nature of solvent strongly affected the extinction coefficients. We may tentatively attribute these changes to slight, solvent-dependent, conformational differences in the chromophore structures that have an effect on the oscillator strength of the S0 → S1.

The absorption spectra of the pure *trans* isomers (Fig. 1a, b, red lines) were obtained by deconvolution of the spectra measured after photoconversion (see below); details of *trans* S0 → S1 in different solvents are also reported in Table 1. For all molecules isomerization to *trans* form led to a well-detectable red shift of the S0 → S1 transition and to a decrease in its extinction coefficient. These findings are consistent with those previously reported for *p*-HBDI and other GFP chromophore analogs (Voliani et al. 2008). Notably, the S0 → S1 transitions of *trans* isomers showed a similar solvent behaviour as their *cis* counterparts (Table 1).

Chromophore photoconversion

Similarly to GFP chromophore analogs in solution (Niwa et al. 1996; Yang et al. 2008; Follenius-Wund et al. 2003), P1-2 and B1-2 showed almost no fluorescence at room temperature ($QY < 10^{-2}$) indicating the presence of very efficient non-radiative deactivation channels of the excited state. The presence of an optical photoconversion channel, eventually identified as *cis-trans* photoisomerization by NMR spectrometry (see below), was assessed in P1-2 and B1-2 by means of laser illumination at 405 nm, i.e. near the S0 → S1 absorption maximum. The photoconversion kinetics was followed either by absorption spectroscopy or by ^{1}H-NMR spectrometry in acetonitrile or d^3-acetonitrile respectively (Fig. 1c). Photoconversion led to an intensity decrease and a detectable red-shift of the S0 → S1 band. The presence of one or more isosbestic points supported the existence of a photoprocess between two optically distinguishable chromophore forms. At long photoconversion times, the absorption spectra displayed almost no changes, suggesting that a photostationary state was reached where the forward and reverse photoconversion rates were the same. When the photosteady state mixture was irradiated at longer wavelength (458 nm), selectively addressing the photoconverted (i.e. the *trans*) form, back-photoconversion took place (Fig. 1d). Back-photoconversion, however, did not completely restore the native chromophore spectrum because a new photosteady state took place. This photosteady state was generated by the residual absorption of *cis* isomer at 458 nm, which implied a non-negligible forward rate.

For each chromophore, the pure molar spectrum of the photoproduct (the *trans* form, A_t) was calculated from the photosteady-state absorption molar spectrum (A_∞), the molar spectrum of the *cis* isomer (A_c), and the NMR-calculated molar fractions of *cis* (x_c) and photoproduct (*trans*, x_t) isomers at photosteady state according to the following equation:

$$A_t = \frac{A_\infty - x_c A_c}{x_t} \quad (1)$$

Notably, the *trans* chromophores at photosteady state were found to decay back negligibly to their *cis* counterparts via thermal mechanisms even at very long times after irradiation. Thermal recovery was monitored by NMR measurements in the dark at 30°C; in all cases thermal recovery kinetics were monoexponential with very long time constants of about 4–5 days ($1/\tau \sim 2\text{–}3{\cdot}10^{-6}$ s^{-1}) for B1. Other chromophores showed comparable or even slower conversion rates.

This photophysical behaviour is consistent with the absence in the chromophores of ionisable residues, differently from *p*-HBDI and consistent with the observed behaviour of T66F GFP chromophore analog (Voliani et al. 2008). Indeed, deprotonation of the phenol group in *p*-HBDI further delocalises electrons over the molecule reducing the energy barrier to the rotation around the exocyclic double bond; removal of ionisable protons hence stabilises the higher-energy *trans* configuration at room temperature (He et al. 2003; Voliani et al. 2008).

Absorption measurements at different times in acetonitrile, together with the spectra of the pure forms, allowed for the determination of the *cis-trans* photoconversion quantum yields (φ_c, φ_t) by using a kinetic model previously described by us (Voliani et al. 2008). Briefly, the model assumes the photoconversion between two ground states with forward (*cis* → *trans*) and backward (*trans* → *cis*) rate constants linearly dependent on illumination intensity and chromophore extinction coefficients. Under the assumption of low optical density (<0.1 Abs) of the solution at all times, the illumination intensity can be considered as time-independent and easily measured after crossing the solution volume. Additionally, in such conditions the solution absorbance at illumination wavelength follows an exponential time-decay law described by:

$$A(t) = A_0\left\{1 + \frac{\alpha\varphi_c(\varepsilon_c - \varepsilon_t)}{\lambda}[\exp(-\lambda t) - 1]\right\} \quad (2)$$

$$\alpha = (\ln 10)\cdot\frac{lP}{V}; \quad \lambda = \alpha(\varepsilon_c\varphi_c + \varepsilon_t\varphi_t) \quad (3)$$

where A_0 is the solution absorption at $t = 0$, V is the solution volume (the solution is irradiated in a rectangular cuvette with l optical path), P is the illumination power (in photon mole/s), and ε_c, ε_t are the extinction coefficients of the *cis* and *trans* isomers at the illumination wavelength

Table 2 Photoconversion quantum yields

	φ_c	φ_t
B1	0.24 ± 0.08	0.38 ± 0.12
B2	0.09 ± 0.04	0.25 ± 0.1
P1	0.16 ± 0.04	0.39 ± 0.09
P2	0.40 ± 0.1	0.18 ± 0.06
p-HMDI (GFP chromophore)[a]	0.21 ± 0.08	0.18 ± 0.02
Y66F GFP chromophore[a]	0.10 ± 0.02	~1

[a] From Voliani et al. 2008

respectively. The reader is referred to our previous paper for further details (Voliani et al. 2008).

Calculated switching yields are reported in Table 2. As already demonstrated for GFP chromophore analogs (Voliani et al. 2008; Yang et al. 2008), the S1 decay channel associated with photoisomerization is particularly effective, as φ_c, φ_t were found to fall in the 0.1–0.4 interval, with $\varphi_c < \varphi_t$: hence out of every 10 absorbed photons, 1–4 would promote photoisomerization. Yet, somewhat surprisingly, the calculated photoswitching yields did not provide evidence of appreciable dependence on the chromophore structure (i.e. butenolide vs. pyrrolinone). This finding adds to the relatively similar switching yields observed for *p*-HBDI and analogs (Voliani et al. 2008; Yang et al. 2008). The presence of electron-donating methoxy groups slightly depressed φ_t, but the effect on φ_c was negative for B2 and positive for P2 (compare B1,P1 with B2,P2 in Table 2). These results should reflect some minor influence of the electronic distribution over the aromatic rings on the conical intersection connecting the two isomerization states.

^{1}H NMR analysis

Monodimensional ^{1}H NMR spectra exhibited the most interesting resonances in the 6.5–9.0 ppm aromatic region. For *cis* chromophores, peak attribution was carried out by considering the predicted chemical shifts and coupling pattern as well as spectra collected on related structures (Fig. 2a, ^{1}H NMR). Protons and peaks were numerically labeled according to the structures of Scheme 1; note that H_4 of B1 and P1 become chemically non-equivalent in B2 and P2, and they are denoted as H_4 and $H_{4'}$.

By inspecting the ^{1}H-NMR spectrum of each chromophore in native *cis* condition and at photosteady state after 405 nm illumination, we found that the photoproduct was inevitably associated with downfield shift of the H_3 proton resonance and a remarkable upfield shift of the H_2 resonance (Fig. 2a). This difference was particularly evident in P1 and P2, where the downfield shift of H_3 was about 0.4 ppm (0.2 ppm in B1 and B2) and the upfield shift of H_2

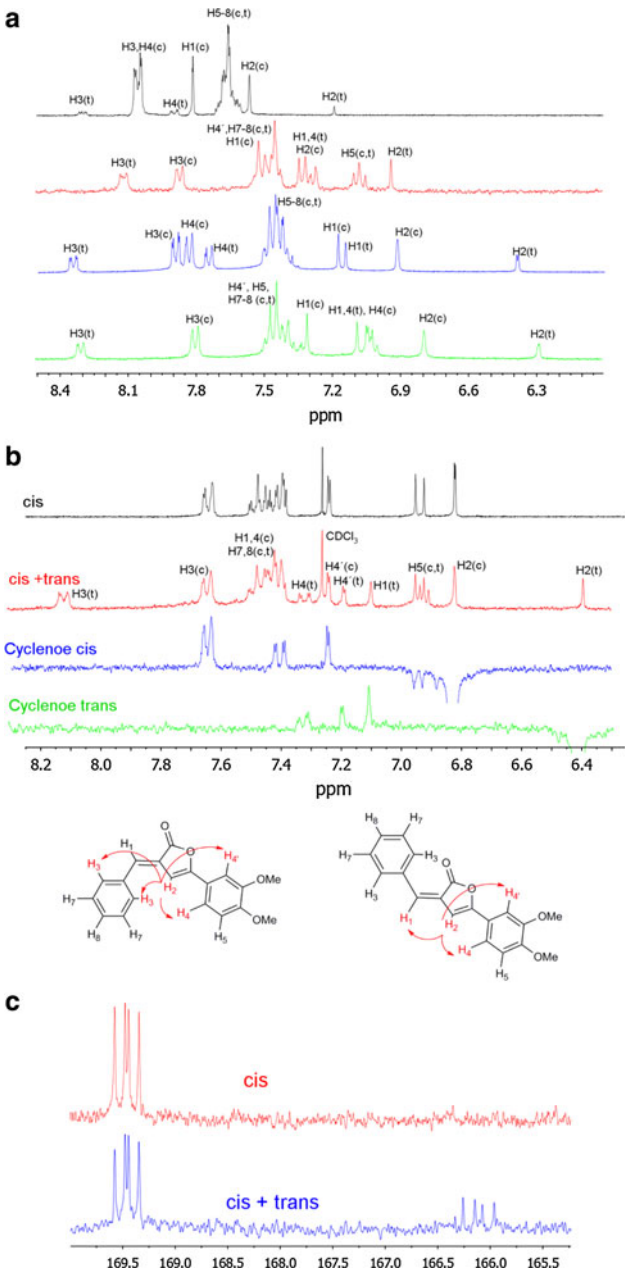

Fig. 2 **a** ^{1}H NMR spectra (DMSO-d_6) of B1 (*black*), B2 (*red*), P1 (*blue*), and P2 (*green*) with assigned peaks, **b** cyclenoe of B2 in $CDCl_3$, **c** coupled ^{13}C NMR spectrum of pure *cis* and *cis* + *trans* B1 (solvent: DMSO-d_6)

was about 0.6 ppm (0.4 ppm for B1 and B2). Notably, we found that all the other aromatic proton resonances were only slightly affected by photoconversion.

The observed changes in the ^{1}H-NMR pattern, particularly at the level of H_2, were exploited to investigate the configurational structure of the chromophores by cyclenoe experiments (Derome 1987). Cyclenoe is a peculiar steady-state measurement of NOE (Derome 1987) based on the subtraction between two monodimensional ^{1}H-NMR spectra. The first of these spectra (sp1) is collected after a saturation pulse in resonance with the nucleus whose surroundings have to be analysed; the second one (sp2) is a ^{1}H spectrum associated with off-resonance saturation pulse. In sp1 the irradiated nucleus resonance vanishes, and NOE is transferred to spatially close nuclei thus modifying their signal intensity (an increase is usually observed in small molecules). Accordingly, s1−s2 results in a spectrum where the irradiated proton resonance is inverted and only those signals belonging to proximal nuclei survive. In our experiments we performed cyclenoe measurements on native and photoconverted chromophores by selectively saturating H_2 resonance attributable to the *cis* or photoproduct structures, which we already described as well-separated (Fig. 2b). We chose to observe the H_2 saturation and the consequent NOE effect on spatially proximal protons because H_2 fills a central position in the molecules (Fig. 2b); hence, cyclenoe was meant to report on the main configurational proton arrangement in the chromophores. Note that cyclenoe measurements were performed in appropriate solvents found to yield a large chemical-shift separation between H_2 resonance and the other protons. This technique proved to be very useful to obtain NOE spectra of the photoproduct even if it was at a low concentration in the mixtures at photosteady state.

In native *cis* structures, NOE was found to deeply affect signals due to protons on the phenyl rings (H_3, H_4, $H_{4'}$) whereas NOE between H_1 and H_2 was never detected. Conversely, in the photoconverted mixtures, the H_3 signal disappeared, the H_1 resonance (singlet, 7.1 ppm) became visible, and the H_4 and $H_{4'}$ remained detectable. These findings can be rationalised by considering that in the native *cis* configuration H_2 is close to H_3, H_4 and $H_{4'}$, whereas in the photoproduct the molecule assumes a different configuration as H_2 is close to H_1, H_4 and $H_{4'}$. As depicted in Fig. 2b, the *trans* configuration accounts properly for the observed NOE effects in the photoproducts. The interaction of both *cis* and *trans* H_2 with both H_4 and $H_{4'}$ strongly suggests that the phenyl ring is freely rotating. Indeed, in the 3,4 disubstituted ring of B2 and P2, H_4 and $H_{4'}$ proton resonances and spectral lines show different chemical shift and structure (H_4 yields a double doublet at 7.4 ppm, whereas $H_{4'}$ is associated with a tight doublet at 7.25 ppm), and none of them disappears in cyclenoe subtraction. This contemporary spatial interaction is consistent with a fast free rotation of the aromatic ring around its 1,4-axis.

^{13}C NMR analysis

^{13}C-NMR helped to unequivocably identify the photoproduct with the *trans* isomer. A great deal of data highlights that $^{3}J_{C,H}$ in the ^{13}C–C=C–H motif is particularly sensitive to the *cis* or *trans* configuration of the double

Table 3 Experimental and calculated $^{3}J_{C\text{-}H}$ (in Hz) coupling constant for four classes of GFP analogs

	B1		P1		Oxazolone		GFP chromophore	
	Cis	*Trans*	*Cis*	*Trans*	*Cis*	*Trans*	*Cis*	*Trans*
Calculated								
H1	7.7	12.8	7.38	11.12	5.39	10.71	5.13	9.41
H2	9.2	7.5	8.21	6.64	–	–	–	–
NH	–	–	2.19	2.31	–	–	–	–
Experimental								
H1	7.4	13.9	7.0	12.7	5.5	12.5	4.4	8.8
H2	9.9	8.5	8.9	7.4	–	–	–	–
NH	–	–	nd	nd	–	–	–	–

bond, with $^{3}J_{C,H}^{trans} > {}^{3}J_{C,H}^{cis}$. In 1975, Vogeli et al. (Vogeli and Philipsborn 1975) systematically investigated vicinal C,H spin coupling in tri-substituted alkenes: for α,β-unsaturated lactones they reported $^{3}J_{C,H}^{cis} = 7.5$ and $^{3}J_{C,H}^{trans} = 14.3$ respectively. Notably this stereospecific effect on $^{3}J_{C,H}$ is enhanced whenever the carbon under observation is unaffected by γ-effect (e.g. a quaternary carbon). Accordingly, we focused our attention on the quaternary carbonylic carbon (resonance around 170 ppm), which is present in all chromophores; this carbon will be henceforth referred to as C_q.

In B1 and B2 we found that C_q coupled with both H_1 and H_2. Nonetheless, $^{3}J_{C,H2}$ is quite similar for both the native *cis* structures and the corresponding photoproducts, being around 9 Hz (Table 3; Fig. 2c). On the other hand, $^{3}J_{C,H1}$ was found to be very different in *cis* isomer ($^{3}J_{C,H1}^{cis} = 7.4$ Hz) and in the photoproduct ($^{3}J_{C,H1}^{trans} =$ 13.9 Hz) (Table 3; Fig. 2c). Under the assumption that photoconversion corresponds to *cis–trans* isomerization, we carried out GIAO/DFT calculations of the $^{3}J_{C,H}$ coupling constants in B1 and P1, and we compared them with the experimental data (Table 3). Our theoretical method was also put to the test by calculating the $^{3}J_{C,H}$ for the *cis* and *trans* isomers of *p*-HBDI and the analog of B1 where the carbon atom in position 4 is replaced by a nitrogen atom. The experimental values of $^{3}J_{C,H}$ for the latter compounds in both *cis* and *trans* form are available from previous reports (Prokofev and Karpeiskaya 1979; Voliani et al. 2008). Excellent agreement between experimental and theoretical values emerged for all compounds for both configurations (Table 3). This finding allowed us to identify the photoconversion process with *cis–trans* photoisomerization; this attribution was also strongly supported by our ^{1}H-NMR cyclenoe measurements. Due to the strict structural homology between the structures examined in this work and the already reported GFP chromophore, the present work is a conclusive validation of the photoinduced conversion from *cis* to *trans* form in GFP-like structures.

An interesting trend can be recognised from the data reported in Table 3. Both *cis* and *trans* $^{3}J_{C,H1}$ gradually decrease upon increasing the substitution of the 5-term ring with heteroatom (N, O). Theoretical calculations, in agreement with experiments, indicate that this behaviour is related to the density of positive charge on the heteroaromatic ring, which decreases with heteroaromatic substitution.

Conclusion

In this work we synthesized four photoswitchable systems sharing a close structural relationship with the GFP chromophore. The selected structures were synthesized in high yields by means of a flexible and straightforward procedure that is insensitive to the nature of the reactants. Hence, future functional derivatives will require only an appropriate choice of the starting reactants and only minor changes of the reaction protocol will be required in order to gain access to suitably functionalized photoswitchable molecular probes. Accurate NMR measurements lead to unambiguous determination of the configuration of the chromophores in both native form and after photoirradiation at absorption maximum. Notably, a precise attribution of NMR signals was performed by means of 1D-NOE experiments, both for the *cis* and for the *trans* isomer. Coupled ^{13}C NMR spectra were collected for selected structures, and comparison with DFT calculations allowed us to establish a strict correlation with the coupling constants of the GFP chromophore. With this correlation, we could further confirm the presence of a *cis-trans* photoisomerization mechanism for the GFP chromophore.

The photophysical examination of the synthesized structures provided evidence of a major red-shift effect (15–40 nm) of the additional phenyl ring on the absorption spectrum compared with GFP chromophore analogs. Indeed, these compounds can be photoaddressed by illumination sources in the visible range of the spectrum, being

therefore much more suitable for applications involving living systems. In accordance with previous results on similar structures, photoconversion quantum yields were found to be usually very high ($\phi > 0.1$). In contrast with the GFP chromophore, however, the thermal decay channel from the high energy *trans* isomer to the *cis* isomer was nearly absent. Taken together these results point out the remarkable purely optical switching control of these new photochromic molecular systems. The absence of reactive sites on the probe makes these structures insensitive to usual physiologic conditions.

Overall, the reported photoswitchable structures possess intriguing photophysical properties and represent promising tools in biophysical research. Further studies are in progress in order to incorporate these structures as switching units in more complex molecular devices for high-resolution imaging of living samples.

Acknowledgments This work was partially supported by the Italian Ministry for University and Research (MiUR) under the framework of the FIRB projects RBLA03ER38 and RBPR05JH2P, and PRIN 2008JZ4MLB_002.

References

Abbruzzetti S, Bizzarri R, Luin S, Nifosi R, Storti B, Viappiani C, Beltram F (2010) Photoswitching of E222Q GFP mutants: "concerted" mechanism of chromophore isomerization and protonation. Photochem Photobiol Sci 9:1307–1319

Ando R, Mizuno H, Miyawaki A (2004) Regulated fast nucleocytoplasmic shuttling observed by reversible protein highlighting. Science 306:1370–1373

Ando R, Flors C, Mizuno H, Hofkens J, Miyawaki A (2007) Highlighted generation of fluorescence signals using simultaneous two-color irradiation on Dronpa mutants. Biophys J 92:L97–L99

Andresen M, Stiel AC, Trowitzsch S, Weber G, Eggeling C, Wahl MC, Hell SW, Jakobs S (2007) Structural basis for reversible photoswitching in Dronpa. Proc Natl Acad Sci USA 104: 13005–13009

Andresen M, Stiel AC, Folling J, Wenzel D, Schonle A, Egner A, Eggeling C, Hell SW, Jakobs S (2008) Photoswitchable fluorescent proteins enable monochromatic multilabel imaging and dual color fluorescence nanoscopy. Nat Biotechnol 26:1035–1040

Betzig E, Patterson GH, Sougrat R, Lindwasser OW, Olenych S, Bonifacino JS, Davidson MW, Lippincott-Schwartz J, Hess HF (2006) Imaging intracellular fluorescent proteins at nanometer resolution. Science 313:1642–1645

Bizzarri R, Serresi M, Cardarelli F, Abbruzzetti S, Campanini B, Viappiani C, Beltram F (2010) Single amino acid replacement makes Aequorea victoria fluorescent proteins reversibly photoswitchable. J Am Chem Soc 132:85–95

Bourotte M, Schmitt M, Follenius-Wund A, Pigault C, Haiech J, Bourguignon JJ (2004) Fluorophores related to the green fluorescent protein. Tetrahedron Lett 45:6343–6348

Cossi M, Barone V (2001) Time-dependent density functional theory for molecules in liquid solutions. J Chem Phys 115:4708–4717

Derome AE (1987) Modern NMR techniques for chemistry research. Pergamon Press, Oxford

Dong J, Abulwerdi F, Baldridge A, Kowalik J, Solntsev KM, Tolbert LM (2008) Isomerization in fluorescent protein chromophores involves addition/elimination. J Am Chem Soc 130:14096–14098

Fernandez-Suarez M, Ting AY (2008) Fluorescent probes for super-resolution imaging in living cells. Nat Rev Mol Cell Biol 9:929–943

Follenius-Wund A, Bourotte M, Schmitt M, Iyice F, Lami H, Bourguignon JJ, Haiech J, Pigault C (2003) Fluorescent derivatives of the GFP chromophore give a new insight into the GFP fluorescence process. Biophys J 85:1839–1850

Frisch MJ, Trucks GW, Schlegel HB, Scuseria GE, Robb MA, Cheeseman JR, Scalmani G, Barone V, Mennucci B, Petersson GA, Nakatsuji H, Caricato M, Li X, Hratchian HP, Izmaylov AF, Bloino J, Zheng G, Sonnenberg JL, Hada M, Ehara M, Toyota K, Fukuda R, Hasegawa J, Ishida M, Nakajima T, Honda Y, Kitao O, Nakai H, Vreven T, Montgomery JJA, Peralta JE, Ogliaro F, Bearpark M, Heyd JJ, Brothers E, Kudin KN, Staroverov VN, Kobayashi R, Normand J, Raghavachari K, Rendell A, Burant JC, Iyengar SS, Tomasi J, Cossi M, Rega N, Millam JM, Klene M, Knox JE, Cross JB, Bakken V, Adamo C, Jaramillo J, Gomperts R, Stratmann RE, Yazyev O, Austin AJ, Cammi R, Pomelli C, Ochterski JW, Martin RL, Morokuma K, Zakrzewski VG, Voth GA, Salvador P, Dannenberg JJ, Dapprich S, Daniels AD, Farkas Ö, Foresman JB, Ortiz JV, Cioslowski J, Fox DJ (2009) Gaussian-09 revision A.1. Gaussian, Wallingford, CT

He X, Bell AF, Tonge PJ (2003) Ground state isomerization of a model green fluorescent protein chromophore. FEBS Lett 549:35–38

Helgaker T, Watson M, Handy NC (2000) Analytical calculation of nuclear magnetic resonance indirect spin-spin coupling constants at the generalized gradient approximation and hybrid levels of density-functional theory. J Chem Phys 113:9402–9409

Hell SW (2007) Far-field optical nanoscopy. Science 316:1153–1158

Hell SW (2009) Microscopy and its focal switch. Nat Methods 6:24–32

Hess ST, Girirajan TP, Mason MD (2006) Ultra-high resolution imaging by fluorescence photoactivation localization microscopy. Biophys J 91:4258–4272

Kojima S, Ohkawa H, Hirano T, Maki S, Niwa H, Ohashi M, Inouye S, Tsuji FI (1998) Fluorescent properties of model chromophores of tyrosine-66 substituted mutants of Aequorea green fluorescent protein (GFP). Tetrahedron Lett 39:5239–5242

Luin S, Voliani V, Lanza G, Bizzarri R, Amat P, Tozzini V, Serresi M, Beltram F (2009) Raman study of chromophore states in photochromic fluorescent proteins. J Am Chem Soc 131:96–103

Niwa H, Inouye S, Hirano T, Matsuno T, Kojima S, Kubota M, Ohashi M, Tsuji FI (1996) Chemical nature of the light emitter of the Aequorea green fluorescent protein. Proc Natl Acad Sci USA 93:13617–13622

Prokofev EP, Karpeiskaya EI (1979) Proton coupled C-13 NMR direct determination of Z-configuration, E-configuration of 4-benzyliden-2-phenyl(methyl)-delta-2-oxazolin-5-ones and products of their solvolysis. Tetrahedron Lett 737–740

Rust MJ, Bates M, Zhuang X (2006) Sub-diffraction-limit imaging by stochastic optical reconstruction microscopy (STORM). Nat Methods 3:793–795

Schueler FW, Hanna C (1951) Unsatured lactones. II. The relationship between chemical constistution and absorption spectra in a group of crotolactones. J Am Chem Soc 73:3528–3530

Schwentker MA, Bock H, Hofmann M, Jakobs S, Bewersdorf J, Eggeling C, Hell SW (2007) Wide-field subdiffraction RESOLFT microscopy using fluorescent protein photoswitching. Microsc Res Tech 70:269–280

Signore G, Nifosi R, Albertazzi L, Bizzarri R (2009) A novel coumarin fluorescent sensor to probe polarity around biomolecules. J Biomed Nanotechnol 5:722–729

Signore G, Nifosi R, Albertazzi L, Storti B, Bizzarri R (2010) Polarity-sensitive coumarins tailored to live cell imaging. J Am Chem Soc 132:1276–1288

Stepanenko OV, Verkhusha VV, Kuznetsova IM, Uversky VN, Turoverov KK (2008) Fluorescent proteins as biomarkers and biosensors: throwing color lights on molecular and cellular processes. Curr Protein Pept Sci 9:338–369

Tripathi AN, Chauhan L, Thankachan PP, Barthwal R (2007) Quantum chemical and nuclear magnetic resonance spectral studies on molecular properties and electronic structure of berberine and berberrubine. Magn Reson Chem 45:647–655

Vogeli U, Philipsborn WV (1975) Vicinal C,H spin coupling in substituted alkenes—stereochemical significance and structural effects. Org Magn Reson 7:617–627

Voityuk AA, Michel-Beyerle ME, Rosch N (1998) Quantum chemical modeling of structure and absorption spectra of the chromophore in green fluorescent proteins. Chem Phys 231:13–25

Voliani V, Bizzarri R, Nifosi R, Abbruzzetti S, Grandi E, Viappiani C, Beltram F (2008) Cis–trans photoisomerization of fluorescent-protein chromophores. J Phys Chem B 112:10714–10722

Yan Y, Marriott ME, Petchprayoon C, Marriott G (2011) Optical switch probes and optical lock-in detection (OLID) imaging microscopy: high-contrast fluorescence imaging within living systems. Biochem J 433:411–422

Yang JS, Huang GJ, Liu YH, Peng SM (2008) Photoisomerization of the green fluorescence protein chromophore and the meta- and para-amino analogues. Chem Commun (Camb) 1344–1346